

## PROPERTIES OF EXTENSIVE AIR SHOWERS \*

MARKUS RISSE

H. Niewodniczański Institute of Nuclear Physics, Polish Academy of Sciences  
Radzikowskiego 152, 31-342 Kraków, Poland

and

Forschungszentrum Karlsruhe, Institut für Kernphysik  
76021 Karlsruhe, Germany

e-mail: markus.risse@ifj.edu.pl

*(Received March 8, 2004)*

Some general properties of extensive air showers are discussed. The main focus is put on the longitudinal development, in particular the energy flow, and on the lateral distribution of different air shower components. The intention of the paper is to provide a basic introduction to the subject rather than a comprehensive review.

PACS numbers: 96.40.Pq, 96.40.-z, 96.40.Tv, 13.85.-t

**1. Introduction**

Extensive air showers (EAS) are known for about 70 years to be cascades initiated by primary cosmic rays in the atmosphere. As such, they serve as connection to the highest particle energies nature is offering, especially at energies exceeding  $10^{15}$  eV where direct measurements of cosmic rays are hampered by the low primary flux. EAS can be viewed as tools for astroparticle physics. The main task is to reconstruct from the shower observables the parameters of the initial cosmic ray, which is in general straightforward for the particle direction. It is more a challenge for the energy and much more for the particle type of the primary. This is due mostly to shower fluctuations, an important EAS property given by the stochastic nature of the elementary interaction processes. Combined with the steep primary spectrum, the fluctuations impose a particular challenge for interpreting air shower data. Use can be made, however, of the fact that an EAS consists of different shower components.

---

\* Presented at the Cracow Epiphany Conference on Astroparticle Physics, Cracow, Poland, January 8-11, 2004.

The main body of this paper deals with illustrating, supported by EAS simulations, some characteristics of these shower components and the information they contain about the primary particle. This might serve as introduction to the subject of extensive air showers and help to better understand what air shower experiments are measuring, which information they try to infer from the data, and where limitations are given [1]. A more comprehensive introduction to EAS is given *e.g.* in [2].

A schematic sketch of an EAS is given in figure 1. The incident particle (primary energy  $E_0$  and primary type  $A_0$ ) hits an air nucleus. Usually considered as extreme illustrations of primary particle types are protons and iron nuclei (although an analysis of EAS data is not restricted to this range). The notation  $A_0$  anticipates the fact that EAS features of primary hadrons, which are known as dominant cosmic rays from direct measurements at energies below  $10^{15}$  eV, show some dependence on the nucleon number  $A$  of a nucleus, as explained later. In the first interaction, a number of secondary hadronic particles are generated. Mostly by decay of the neutral pions, electromagnetic sub-cascades are initiated, and by decay of (part of) the charged pions, muons and neutrinos are produced. While neutrinos are hardly detectable in classic air shower experiments, muons might reach the observation level even from large altitudes. It is important to note that a competition of the charged pions between decay and interaction exists which depends on the pion energy and the local air density. Some information on the first interactions will be imprinted in this way in the muon component. The remainder of the hadronic secondaries continues to interact with air in subsequent collisions and to feed the other shower components.

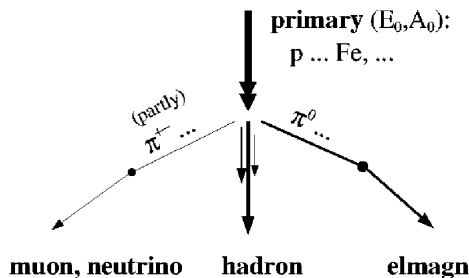


Fig. 1. Schematic sketch of an EAS.

In ground arrays, the surviving particles are measured with particle detectors, and with appropriate optical telescopes Cherenkov and fluorescence emission during the shower propagation can be observed.

To characterize more quantitatively the interaction process, it is helpful to introduce the quantity *inelasticity*  $k$  as the energy fraction available for

the production of secondary particles (or in other words, the initial collision energy reduced by the energy of the most energetic particle). As a rule of thumb, about  $\frac{1}{3}k$  is “lost” to the electromagnetic channel per hadronic interaction. For a mean value  $k \simeq 0.6$  typical for high-energy interactions this corresponds to  $\simeq 20\%$  per interaction that on average will give rise to subsequent electromagnetic cascading. Equipped with this knowledge, we can turn to the longitudinal shower development.

## 2. Longitudinal shower development

### 2.1. Energy flow

At first the general energy flow in an air shower is discussed in some detail. In figure 2, the energy carried by different shower components during the cascade development are displayed for the example of a proton-induced event of primary energy  $10^{19}$  eV. These are results of detailed Monte Carlo air shower simulations obtained with the program package CORSIKA [3]. For more information on simulation in particular at the highest energies, see for instance [4] and references given therein.

Initially, all energy is concentrated in the primary proton. For this event, the first interaction occurs after traversing an atmospheric depth of  $\simeq 40$  g cm $^{-2}$ . A significant energy fraction is transferred to the electromagnetic component, which is further fed in the subsequent shower process. One can notice an exponential decrease of the energy left in the hadrons. This can be understood in a simple picture of a constant inelasticity  $k$  and a constant mean free path  $\lambda_h$  for hadronic interactions. Based on the average fraction of  $\frac{1}{3}k$  that is put into electromagnetic channel per hadronic interaction, the energy remaining in the hadronic component at depth  $X$  is

$$E_h(X) = E_0 \left(1 - \frac{1}{3}k\right)^{X/\lambda_h}. \quad (1)$$

Adopting typical values used for modeling nucleon–air interactions at high energies of  $\lambda_h \simeq 55$  g cm $^{-2}$  and  $k \simeq 0.6$ , the hadronic scale depth  $A_h$  of the exponential fall-off thus amounts to

$$A_h = \frac{\lambda_h}{\left|\ln\left(1 - \frac{1}{3}k\right)\right|} \simeq 250 \text{ g cm}^{-2} \quad (2)$$

in reasonable agreement with the results plotted for the detailed simulation.

In this approximation, energy losses into the muon and neutrino channels were assumed to be small. In fact, as can be seen only at later stages of the shower development, an energy fraction of around 5% of the initial energy has accumulated in these components. The different character of the

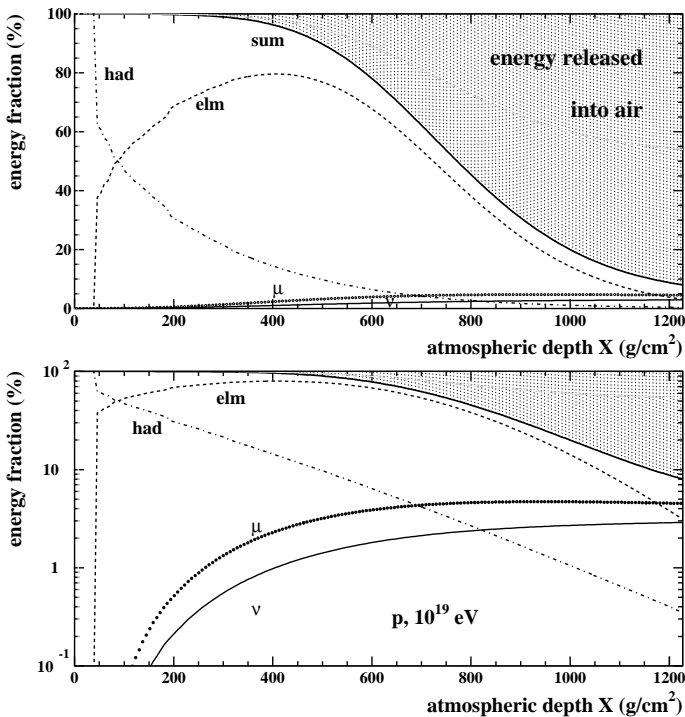


Fig. 2. Energy flow in EAS as obtained by CORSIKA shower simulations for an individual  $10^{19}$  eV primary proton event. The energy fractions stored in hadrons, electromagnetic particles, muons, and neutrinos are shown. The difference between their sum to the initial energy indicates the total amount of energy already released into air (shaded area). Upper graph in linear, lower graph in logarithmic scale.

longitudinal curves of these two components with respect to hadrons and electromagnetic particles is evident. It is an important feature of muons to transport most of their (though small) energy fraction down to observation level.

The electromagnetic particle channel is rising fast. The process to extract energy from the electromagnetic particles is the energy loss due to ionization of air induced by the charged shower particles [5]. Therefore, in figure 3 the number of shower electrons (a term which usually includes positrons) is overlayed to the previous energy flow plot. Since the specific ionization loss  $\alpha$  of relativistic electrons is about constant ( $\alpha \simeq 2 \text{ MeV}/(\text{g cm}^{-2})$ ), the same curve in appropriate units also resembles the differential energy release

$dE_{\text{rel}}(X)/dX$  of the EAS as a whole,

$$\frac{dE_{\text{rel}}}{dX}(X) \simeq \alpha N(X). \quad (3)$$

Integrating  $dE_{\text{rel}}(X)/dX$  results in the energy fraction indicated by the shaded region; for instance, at shower maximum (labeled  $X_{\text{max}}$ ), already  $\simeq 50\%$  of the initial energy has been released into the atmosphere.

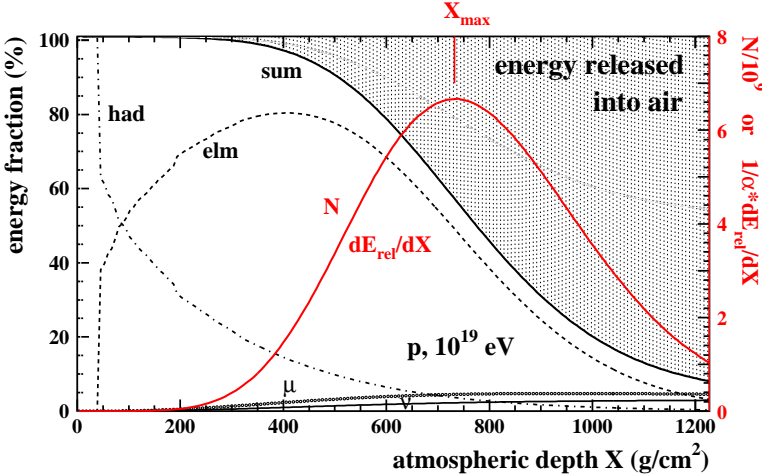


Fig. 3. Energy flow in EAS (left scale, compare Fig. 2) and cascade profiles  $N(X)$  or  $1/\alpha \cdot dE_{\text{rel}}(X)/dX$  (right scale). The depth where the shower reaches its maximum number of particles is indicated by  $X_{\text{max}}$ .

The maximum of energy stored in electromagnetic particles  $X_{\text{elm}} \simeq 410 \text{ g cm}^{-2}$  is reached well before the so-called shower maximum  $X_{\text{max}} \simeq 730 \text{ g cm}^{-2}$ , *i.e.* the depth where the shower contains the largest electron multiplicity. This is due to the fact that at early cascade stages, a large energy fraction is carried by high-energy particles. Only gradually, the energy is transformed to newly created particles. The maximum of energy stored in electromagnetic particles  $X_{\text{elm}}$  is expected at the development stage where the gain from the hadron channel equals the loss by energy release,

$$-\frac{dE_{\text{had}}}{dX}(X_{\text{elm}}) \simeq \frac{dE_{\text{rel}}}{dX}(X_{\text{elm}}). \quad (4)$$

We can roughly cross-check  $X_{\text{elm}}$  in our simplified approach. Using Eq. (3) and (by differentiating Eq. (1))  $-dE_h(X)/dX \simeq E_h(X)/\Lambda_h$  we obtain from Eq. (4) for  $X_{\text{elm}}$  the condition

$$E_h(X_{\text{elm}}) \simeq \alpha \Lambda_h N(X_{\text{elm}}). \quad (5)$$

Adopting (rounded) values yields an expectation of  $E_h(410 \text{ g cm}^{-2}) \simeq 2 \times 250 \times 2 \times 10^9 \text{ MeV} = 10\% \times E_0$  which is in reasonable agreement with the data.

Equations (4) and (5) indicate the connection between energy flow (of hadron to electromagnetic channel) and particle multiplication (in the electromagnetic channel). Most important for the observation are the profiles  $dE_{\text{rel}}(X)/dX$  or  $N(X)$ , respectively. These profiles are observable as fluorescence light and indicate how many particles reach the observation level. We therefore next investigate some characteristics of cascade curves formed by particle multiplication.

### 2.2. Profile features

Some of the main features of shower profiles can be nicely motivated within a simple toy model of particle cascades [6], which complements to the previous toy model of energy flow. Let us suppose a particle with energy  $E_0$  that splits its energy equally into two particles after traveling a path-length  $\lambda$ , and let this process be repeated by the secondaries. We then obtain a particle cascade which at a path-length  $X$  has evolved into  $N(X) = 2^{X/\lambda}$  particles of equal energy  $E(X) = E_0/N(X)$ . Let us further assume that particle multiplication stops when a certain energy limit  $E = E_l$  is reached. Then, the maximum number of particles  $N_{\text{max}}$  is reached at this point  $X_{\text{max}}$ , and it is given by  $N_{\text{max}} = N(X_{\text{max}}) = E_0/E_l$ . The position of  $X_{\text{max}}$  follows as  $X_{\text{max}} = \lambda/\ln 2 \times \ln(E_0/E_l)$ .

Within this toy model, let us construct the more general case of an initial set  $(A_0, E_0/A_0)$  of  $A_0$  particles, each with energy  $E_0/A_0$ . (The previous case is then realized for  $A_0 = 1$ .) The particle number at maximum and the position of shower maximum are then given by

$$N_{\text{max}}(A_0, E_0/A_0) = N_{\text{max}}(E_0) \propto E_0, \quad (6)$$

$$X_{\text{max}}(A_0, E_0/A_0) \propto \ln(E_0/A_0 E_l) \leq X_{\text{max}}(E_0). \quad (7)$$

If we identify the initial particle set  $(A_0, E_0/A_0)$  as primary nucleus of mass number  $A_0$  (this is known as ‘‘superposition model’’), the toy model predictions can thus be summarized as:

- $N_{\text{max}}$  increases proportional to the primary energy;
- $N_{\text{max}}$  is the same for all nuclei;
- $X_{\text{max}}$  increases with the logarithm of the primary energy;
- $X_{\text{max}}$  is smaller for the heavier nuclei (logarithmic dependence on  $A_0$ );
- $X_{\text{max}}$  is the same for same  $E_0/A_0$  but different  $E_0$ .

Despite the obvious simplicity (and its limitations) of this toy model, the findings of detailed shower simulations are quite well reproduced, as illustrated in figures 4 and 5: The average  $X_{\max}$  increases with  $\ln E_0$  and is smaller for primary iron ( $A_0 = 56$ ) compared to primary proton, with a difference of  $\simeq 80\text{--}100\text{ g cm}^{-2}$  (Fig. 4). The primary iron  $X_{\max}$  for  $E_0$  fits well to the proton one of energy  $E_0/56$  (same  $E_0/A_0$ ).  $N_{\max}$  is quite similar for the different primaries (Fig. 5) and about proportional to  $E_0$  (not shown).

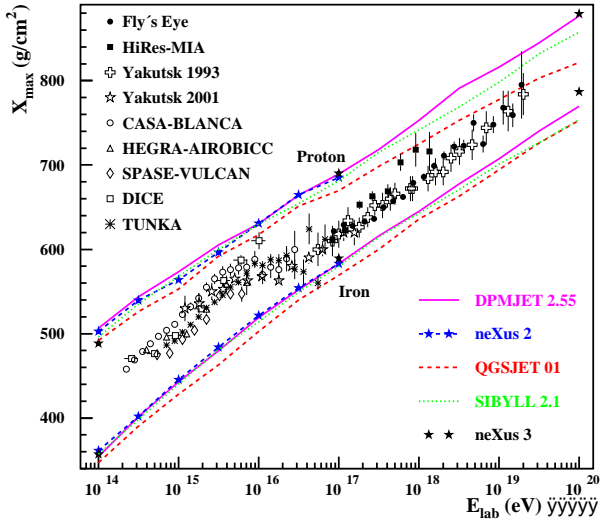


Fig. 4. Average depth of shower maximum as a function of primary energy [7].

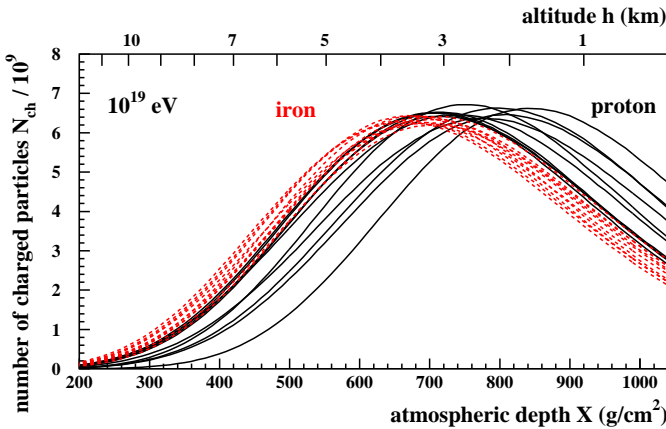


Fig. 5. Individual longitudinal shower profiles (vertical incidence).

Two other important EAS properties should be pointed out from Fig. 5. Firstly, for fixed  $E_0$  different  $X_{\max}$  values translate into different particle numbers on ground. For instance, the primary proton showers result on average in a larger number of ground particles compared to iron showers if the observation level is beyond the maximum. Thus, observation of  $X_{\max}$  or related quantities provide information on the primary particle type. Secondly, however, shower-to-shower fluctuations are visible, that lead to partly overlapping distributions of shower observables. As an example, the  $\text{RMS}(X_{\max})$  of primary protons is  $\simeq 60 \text{ g cm}^{-2}$  and thus nearly as large as the difference between the average values of proton and iron. This limits an event-by-event assignment of a primary particle type, and composition analyses are usually performed with large event samples. However, it can also be seen that iron shower fluctuations are smaller (*e.g.*  $\text{RMS}(X_{\max}) \simeq 20 \text{ g cm}^{-2}$ ) than the proton ones. This might be used in turn to conclude about the primary composition by studying the very fluctuations of shower observables in a given event sample.

### 2.3. Shower electrons and muons

The total number of shower particles regarded so far was dominated by the shower electrons. The shower muons, however, provide complementary information on the primary particle. As visible from the longitudinal distributions in figure 6 (top), the muon particle number is decreasing only slowly after the maximum, in contrast to the shower electrons. Moreover, the total muon number also depends on the primary particle type. In the superposition model, the larger total muon content in iron showers might be qualitatively understandable: Due to the smaller energy per nucleon ( $E_0/A_0$ ), the secondary pions are less energetic. This favours a pion decay as well as the fact that iron events develop at larger altitudes, where the air density is smaller.

Shown in figure 6 (bottom) are muon *versus* electron number for proton and iron induced events for different fixed primary energies. The size of each “potato” corresponds to the shower fluctuation, while the separation indicates that a correlated measurement of ground particle numbers of shower electrons and muons allows conclusions on the primary mass.

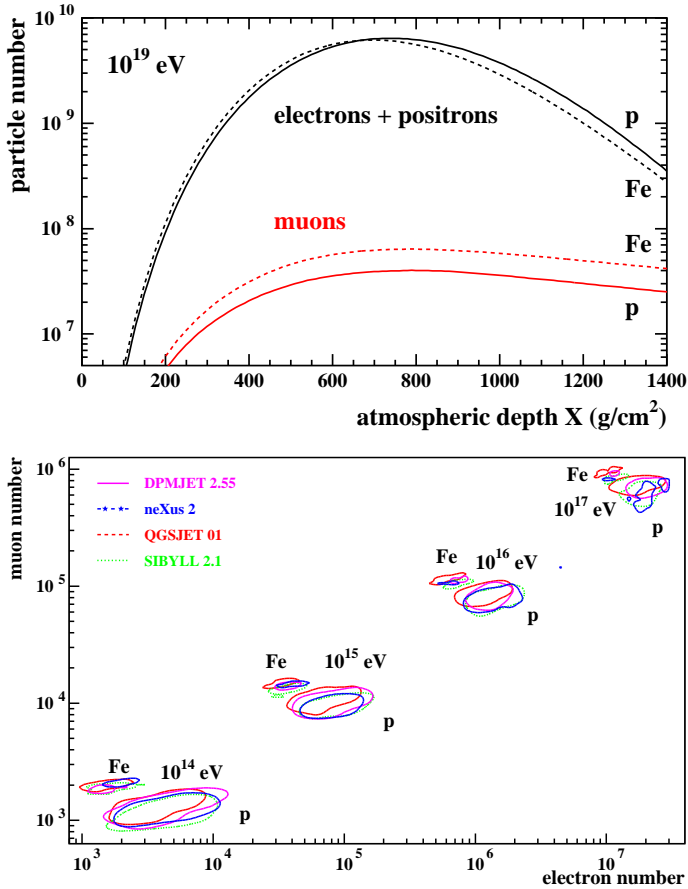


Fig. 6. Top: Longitudinal profiles of typical primary proton and iron events for shower muons and electrons. Bottom: Distribution of total muon and electron number on ground for proton and iron induced showers of different primary energies [8].

### 3. Lateral distribution

Only the longitudinal development was discussed so far. Air showers have a lateral spread that also differs for the different shower components as well as for the various primary particles. It can be seen in figure 7 (top) that the lateral distribution of shower muons on ground is flatter than the distribution of shower electrons. This is mostly due to the muon origin from larger altitudes compared to the more local production and fading of the electron component. In spite of the electrons being much more numerous than muons (about two orders of magnitude around shower maximum, see Fig. 6), at larger distance from the shower core the particle densities become comparable.

Given the differences in the longitudinal development between primary proton and iron events, differences also in the lateral distributions might be expected. In figure 7 (bottom), the ratio of particle densities of proton-induced to iron-induced events is displayed for shower muons and electrons. Both ratios decrease with increasing distance from the shower centre, indicating the flatter lateral distributions in case of the (on average) more developed primary iron showers. The larger muon content of iron-induced events is also visible (ratio  $< 1$ ). The larger electron number on ground for primary proton showers can now be specified as larger ground particle density closer to the core, while at larger distances (which contribute less to the integrated, total particle number), the electron density in iron events is larger due to the flat lateral distribution. Thus, measuring local particle densities of the different shower components as a function of core distance provides additional information on the primary particle, which is utilized in large arrays of ground particle detectors.

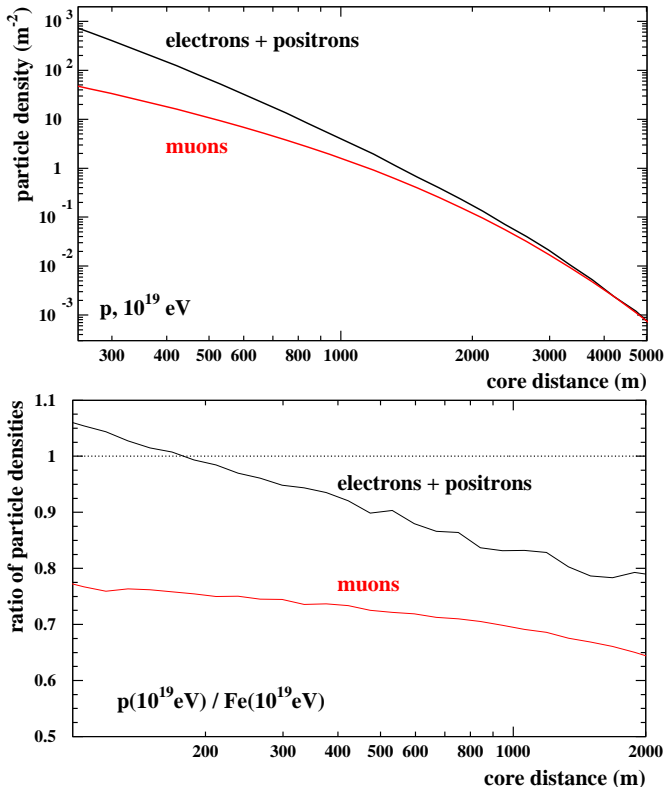


Fig. 7. Top: Lateral distribution on ground of shower muons and electrons. Bottom: Ratio of lateral distributions on ground in proton to iron induced events, both for shower muons and electrons.

#### 4. Discussion and conclusion

Extensive air showers consist of different particle components which have different shower characteristics. This gives a handle to determine primary energy and (to some extent) the primary particle type. Extensions of this approach that were not discussed comprise the exploitation of different time structures of the shower front or comparing inclined events (where mostly muons survive the increased atmospheric path-length) to near-vertical ones. Also in the hadronic shower component, information on the primary particle type is imprinted; but maybe even more important is the possibility to test high-energy hadronic interaction models used in the simulations. Shower simulations have grown to an important tool for EAS data reconstruction. Shower fluctuations motivate the development of Monte Carlo simulation techniques. In turn, these simulations might also be applied to find observables that depend less strongly on the specific primary or on shower fluctuations, such as the signal at distances of 600–1000 m from the core for primary energy estimations with ground arrays. At the highest energies, further interaction features have to be considered in shower simulations, *e.g.* for primary photons the LPM effect and preshower formation in the geomagnetic field.

In summary, even after many years of extensive exploration, air showers continue to be fascinating tools for astroparticle physics.

The conference organizers are thanked for their kind hospitality and for creating an inspiring conference atmosphere. In particular, I would like to thank Marek Jeżabek and Henryk Wilczyński — dziękuję bardzo! The fruitful collaboration with Ralph Engel and Dieter Heck is gratefully acknowledged. The author is supported by the Alexander von Humboldt Foundation.

#### REFERENCES

- [1] See the various contributions in these proceedings.
- [2] T.K. Gaisser, *Cosmic Rays and Particle Physics*, Cambridge University Press, Cambridge 1990.
- [3] D. Heck, J. Knapp, J.N. Capdevielle, G. Schatz, T. Thouw, FZKA 6019, Forschungszentrum Karlsruhe 1998; [www-ik.fzk.de/~heck/corsika](http://www-ik.fzk.de/~heck/corsika).
- [4] J. Knapp, D. Heck, S.J. Sciutto, M.T. Dova, M. Risse, *Astropart. Phys.* **19**, 77 (2003).
- [5] M. Risse, D. Heck, *Astropart. Phys.* **20**, 661 (2004).
- [6] W. Heitler, *Quantum Theory of Radiation* (2nd Ed.), Oxford University Press, Oxford 1944.
- [7] D. Heck, M. Risse, J. Knapp, *Nucl. Phys. (Proc. Suppl.)* **B122**, 364 (2003).
- [8] D. Heck *et al.*, KASCADE Collaboration, Proc. 27<sup>th</sup> Int. Cosmic Ray Conf., p. 233, Hamburg 2001.